Probing the Molecular and Electronic Structure of Capsaicin: A Spectroscopic and Quantum Mechanical Study

A. Alberti,[†] V. Galasso,*[,‡] B. Kovač,[§] A. Modelli,[||,⊥] and F. Pichierri[#]

ISOF, Area della Ricerca del CNR, via Gobetti 101, I-40129 Bologna, Italy, Dipartimento di Scienze Chimiche, Università di Trieste, I-34127 Trieste, Italy, The Ruđer Bošković Institute, HR-10002, Zagreb, Croatia, Dipartimento di Chimica G. Ciamician, Università di Bologna, I-40129 Bologna, Italy, Centro Interdipartimentale di Ricerca in Scienze Ambientali, Università di Bologna, I-48100 Ravenna, Italy, and Department of Applied Chemistry, Graduate School of Engineering, and Global COE, Tohoku University, Aoba-yama 6-6-07, Sendai 980-8579, Japan

Received: March 4, 2008; Revised Manuscript Received: April 2, 2008

The conformational preferences of capsaicin were investigated by using the hybrid meta density functional theory (DFT) method MPWB1K. Its flexible, pendant side chain allows for a multitude of conformations only slightly different in energy. The distinctive vibrational features of the most stable conformers were characterized. To elucidate the most favorable reaction sites of capsaicin for radical scavenging, various homolytic bond-dissociation energies were also calculated. Of the possible radical intermediates, the allyl and benzyl radicals are energetically preferred. The filled and empty electronic structures of capsaicin were investigated by exploiting the photoelectron and electron-transmission spectra also of reference molecules and suitable quantum-mechanical calculations. On this basis, a reliable pattern of the vertical ionization energies and electron-attachment energies of capsaicin was proposed. The frontier π molecular orbitals are concentrated over the vanillyl moiety, with a modest influence of the amidic−aliphatic chain. The (negative) first vertical electron affinity is predicted to be similar to that of benzene. The absorption spectrum of capsaicin and its change by conversion into a phenolic deprotonated anion (modest bathochromic displacement) or a phenoxyl neutral radical (from colorless to red) were interpreted with time-dependent DFT calculations. ESR measurements following chemical or electrochemical reduction of capsaicin did not lead to detection of the corresponding radical anion. The spectra show fragmentation of the original molecule and formation of a variety of radical species which are believed to have a semiquinonic structure.

Introduction

Natural phenolic compounds have attracted a great deal of interest owing to the positive effects connected to their biochemical properties, such as antioxidative, radical scavenging, anti-inflammatory, antidepressant, and assumed cancer-preventive effects.[1] Among these organic natural products, capsaicin (**CA**), the major component of the hot chili pepper fruits (*Capsicum* spp.), is one of the most exploited biomolecules. In this regard, recent electrophysiology experiments indicate that the coadministration of a lidocaine derivative (QX314) and **CA** produces the blockage of sodium channels with a long-lasting decrease of pain sensitivity.[2] However, in the light of its complex and seemingly conflicting activities (including tumorigenic and mutagenic effects), **CA** has also been referred to as a double-edged sword.[3]

CA is an amphiphilic molecule (Figure 1). Indeed, its structure is composed of a hydrophilic aromatic ring (A region), a dipolar amide (B region), and a lipophilic (hydrophobic) octanyl side chain (C region). Previous structure−activity relationship studies of **CA** analogues have shown that each region makes an implicit contribution to activity.[4,5] In this regard, Lambert and Sum[6] have recently reported a molecular dynamics study of the properties of **CA** in

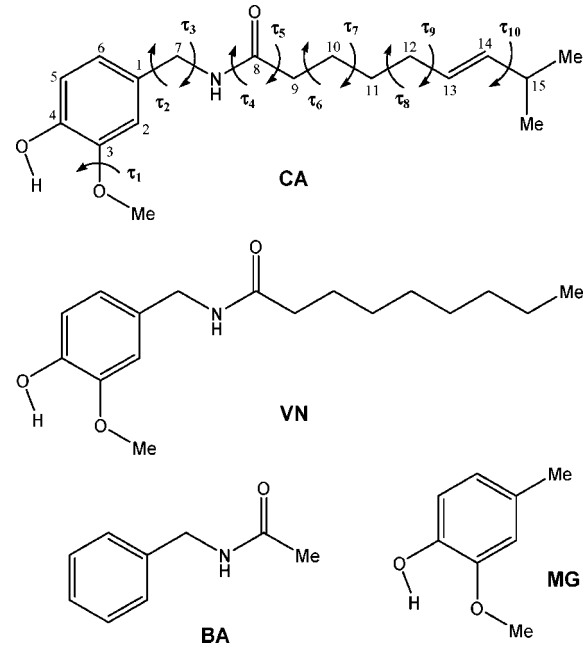

Figure 1. Molecular formulas and labelling.

* To whom correspondence should be addressed. E-mail: galasso@univ.trieste.it.
[†] Area della Ricerca del CNR.
[‡] Università di Trieste.
[§] The Ruđer Bošković Institute.
[||] Dipartimento di Chimica G. Ciamician, Università di Bologna.
[⊥] Centro Interdipartimentale di Ricerca in Scienze Ambientali, Università di Bologna.
[#] Tohoku University.

10.1021/jp801890g CCC: $40.75
Published on Web 05/29/2008

an 1-octanol/water system, aimed at understanding its behavior in biological systems.

On the other hand, no quantum-mechanical study on the conformational preferences and spectroscopic properties of **CA** has been reported so far. The bottleneck for such type of study is the flexibility of the **CA** side chain that generates a potential-energy landscape with a large number of relative minima. This causes the presence of many conformers in both the gas and solution phases, at variance from the solid state, where the various internal degrees of freedom of **CA** are frozen and one definite molecular crystal structure has been experimentally determined by David et al.[7] Interestingly, in the crystal unit cell, four **CA** molecules form a tetramer which is stabilized by intermolecular hydrogen bonds involving their amide moieties and only two hydroxyl groups. In any case, the elucidation of the conformational and electronic properties of **CA** is fundamental to the understanding of its many bioactivities. Thus, the vertical ionization and electron-attachment energies and the electronic transitions of **CA** have been studied with the support of ab initio and density functional theory (DFT) calculations and experimental results obtained for simple reference molecules. An ESR study of the species resulting from its chemical or electrochemical reduction has also been carried out. These complementary data give valuable information, especially about the energy and nature of the frontier molecular orbitals (MOs) that are primarily involved in the biochemical reactivity of **CA**.

Experimental and Computational Details

Preliminary molecular mechanics calculations were performed by using the Cornell version of the Amber force field[8] (at a final energy gradient of 10^{-3} kcal mol^{-1} Å^{-1}) and randomly varying the multitorsional space of the **CA** molecule with the genetic algorithm of Judson and Rabitz.[9] All these semi-empirical calculations were carried out with the Sybyl 7.0 software.[10]

The first 20 lower-energy conformations of **CA** generated in this way were used as the starting structures for high-level DFT calculations. Geometry optimizations were carried out by using the hybrid meta DFT method MPWB1K of Zhao and Truhlar[11] in combination with the 6-31+G(d,p) basis set that performs well for weak interactions and hydrogen bonding. Harmonic-frequency calculations were performed for all the optimized structures to establish that the stationary points are minima. The vibrational characterization was based on the normal-mode analysis performed according to the Wilson FG matrix method[12] by using standard internal coordinates. To ameliorate the agreement between calculated and experimental vibrational frequencies, use was made of a set of scaling factors obtained by empirically fitting the vibrational frequencies of the related simple fragment molecules, phenol,[13a] *trans*-*N*-methyl-acetamide,[13b] and *trans*-2-butene.[13c] (These scaling factors are given in the Supporting Information.)

As to the reference molecules *N*-benzylacetamide (**BA**), *p*-methyl-guaiacol (**MG**), and *N*-vanillylnonanamide (**VN**), a preferred conformation of **BA** was obtained with a DFT optimization of the X-ray molecular crystal structure,[14] the lowest-energy geometry of **MG** was determined by a full conformational search at the DFT level, and one favorable conformation of **VN** was DFT-calculated starting from the most preferred conformation of the parent **CA**.

The vertical E_is of **CA** and of the reference molecules **BA**, **MG**, and **VN** were calculated at the ab initio level with the outer-valence-Green's-function (OVGF) method[15] by using electron propagator techniques[16] and selected according to approximation B.[17] In order to calculate the self-energy part, all occupied valence MOs and the 70 (**MG**), 80 (**BA**), 155 (**VN**), and 160 (**CA**) lowest virtual MOs were considered. The OVGF calculations were performed by using the TZV basis set.[18]

Vertical $S_n \leftarrow S_o$ excitation energies and oscillator strengths were calculated with the TD-DFT method,[19] by employing the B3LYP functional and the cc-pVDZ basis set.[20] Solvent effects were accounted for with the polarizable continuum model (PCM).[21]

The hyperfine coupling constants (HFCCs) were calculated by using the DFT/B3LYP method and the EPR-II basis set.[22]

All quantum-mechanical calculations were performed with the Gaussian 03 software package.[23]

The He(I) photoelectron (PE) spectra were recorded on a Vacuum Generators UV-G3 spectrometer[24] with a spectral resolution of 25 meV when measured at the full width at half maximum of the Ar^+ $^2P_{3/2}$ calibration line. The sample inlet temperatures required to generate sufficient vapor pressure were 80, 30, 180, and 170 °C, for **BA**, **MG**, **VN**, and **CA**, respectively. The energy scale was calibrated by admitting small amounts of Ar and Xe to the sample flow.

The vertical attachment energies (VAEs) of the reference molecules **BA** and **MG** were measured by means of ETS. Our experimental setup is in the format devised by Sanche and Schulz[25] and has been previously described.[26] To enhance the visibility of the sharp resonance structures, the impact energy of the electron beam is modulated with a small ac voltage, and the derivative of the electron current transmitted through the gaseous sample is measured directly by a synchronous lock-in amplifier. Because electron attachment is rapid with respect to nuclear motion, temporary anions are formed in the equilibrium geometry of the neutral molecule. The impact electron energies at which electron attachment occurs are properly denoted as VAEs and are the negative of the vertical electron affinities. Each resonance is characterized by a minimum and a maximum in the derivative signal. The energy of the midpoint between these features is assigned to the VAE. The spectra were obtained in the high-rejection mode[27] and are therefore related to the nearly total scattering cross-section. The electron beam resolution was about 50 meV (fwhm). The energy scale was calibrated with reference to the $(1s^12s^2)^2S$ anion state of He. The estimated accuracy of the measured VAEs is ± 0.05 or ± 0.1 eV, depending on the number of decimal digits reported.

ESR spectra were recorded on an upgraded ER200D/ESP 300 BRUKER spectrometer equipped with a dedicated data station, an NMR gaussmeter for the calibration of the magnetic field, and a microwave frequency counter for the determination of the *g* factors that were corrected with respect to that of the perylene radical cation in concentrated sulfuric acid (2.0025_8). The apparatus for in situ electrochemical reduction consisted of a flat cell (50 × 10 × 0.15 mm) equipped with a platinum gauze (cathode) and a platinum wire (anode) connected to an AMEL potentiostat. This set up only allows the reduction to be carried out at room temperature and does not provide knowledge of the actual applied potential because of the lack of a reference electrode. In a typical experiment, the electrolytic cell was filled with a DMSO solution of either **CA** or **VN** containing Bu_4NBH_4 as supporting electrolyte, and the solution was carefully purged with argon. The applied potential was increased in steps of 0.1 V until a signal was detected. The chemical reduction was attempted with four methods: (i) by mixing thoroughly deoxygenated DMSO solutions of either **CA** or **VN** and potassium *tert*-butoxide in a flat cell; no variations were observed when replacing the flat cell with a capillary tube (i.d. 1 mm); (ii) by

TABLE 1: Relative Energies (kcal mol^{-1}), Torsion Angles (deg), and Dipole Moments (Debye) of CA Conformers in Vacuo

conformer	ΔE	τ_1	τ_2	τ_3	τ_4	τ_5	τ_6	τ_7	τ_8	τ_9	τ_{10}	μ
X[a]		6.6	19.6	−100.8	−168.0	−136.7	77.5	158.5	164.2	−144.7	141.6	
1	0	−0.1	−69.0	93.1	−177.8	137.4	−67.3	−178.1	−62.5	−118.3	1.0	2.43
2	0.02	−76.5	−112.0	−99.6	173.8	−38.8	−59.9	158.1	−75.6	111.4	−5.1	5.44
3	0.06	−5.5	50.2	−99.2	177.5	−153.3	65.2	178.3	−177.9	−123.0	117.2	3.35
4	0.25	−2.6	−72.7	91.2	−169.9	82.2	65.2	−175.4	67.7	−121.3	−0.2	1.89
5	0.25	−5.8	74.4	−89.2	−8.9	−85.4	−69.2	174.5	−69.5	117.3	−1.3	1.64
6	0.28	−6.6	−74.0	88.4	−168.6	87.2	69.7	−174.6	69.9	−115.5	2.6	1.63
7	0.30	9.9	73.9	−89.5	171.0	−89.5	−71.4	175.1	−70.3	115.9	−4.9	1.64
8	0.33	0.9	−70.0	89.1	−166.8	104.2	−179.6	178.0	−65.3	116.4	−1.0	2.33
9	0.36	8.1	110.7	98.4	−175.8	45.0	57.6	−159.3	74.7	−114.7	7.1	5.44
10	0.74	0.7	72.9	−91.4	171.9	−90.2	−67.1	178.8	175.3	121.4	0.3	2.32

[a] Molecular crystal structure, reference (7).

allowing the contact between THF solutions of the substrates containing a small amount of dibenzo-18-crown-6-ether carefully degassed through repeated freeze-and-thaw cycles and a sodium mirror; (iii) by photolyzing in situ (with the light from a 1 kW mercury lamp) a nitrogen-purged solution of **CA** (**VN**) in an EtOH/DME solution containing some sodium ethoxide; and (iv) by adding a small amount of **CA** (VN) to a DMSO solution of potassium superoxide (0.15 M) and dibenzo-18-crown-6-ether (0.30 M). The experimental spectra were computer-simulated by using a custom-made software based on a Monte Carlo minimization procedure.[28]

All chemicals but **BA** were obtained from commercial sources and used as received, including solvents that were stored over activated molecular sieves.

Results and Discussion

Conformational, Energetic, and Vibrational Features. The molecular shape of **CA** can be described as a dish (the aromatic moiety) provided with a long curled stick (the side chain). **CA** has 10 main torsion angles, as shown in Figure 1, that give rise to a multitude of conformational isomers. Schematically, the aromatic part of the molecule is kept frozen, and the methoxy group and the flexible side chain are allowed to rotate in a variety of ways.

In the solid state, the **CA** molecule adopts an approximately planar arrangement, except for the terminal isopropyl group and the H—N—C═O amidic unit that are nearly orthogonal to the average plane. The long chain is curled around the aromatic moiety. This conformation is likely to arise from the absence of solvent molecules in the crystal and from the favored molecular packing. In the gas phase (as well as in solution), the internal degrees of freedom go into action. and the molecular framework spreads out in space. Indeed, the stick of the various conformers exhibits a large deviation from the phenolic plane; as an example, the atoms C_{11} and C_{12} lie 3.61 and 4.14 Å, respectively, above that plane in conformer **1**. Furthermore, there is only a partial resemblance among the conformers. The main differences stem from the steric disposition of the methoxy group and the stick.

The DFT/MPWB1K values of the torsion angles and the energies relative to the most stable conformer are reported in Table 1 for a selection of optimized structures. For comparison, the torsion angles of the crystal structure of **CA**, determined from powder diffraction data by David et al.,[7] are also listed. Figure 2 shows this molecular crystal structure and the DFT geometry of the two lowest-energy conformers in vacuo (**1** and **2**). Notably, the methoxy group is almost coplanar with the phenolic ring in both the solid phase and conformer **1**, whereas it is twisted by 77° in conformer **2**. (Tables containing the Cartesian coordinates of these two conformers are given in the Supporting Information.)

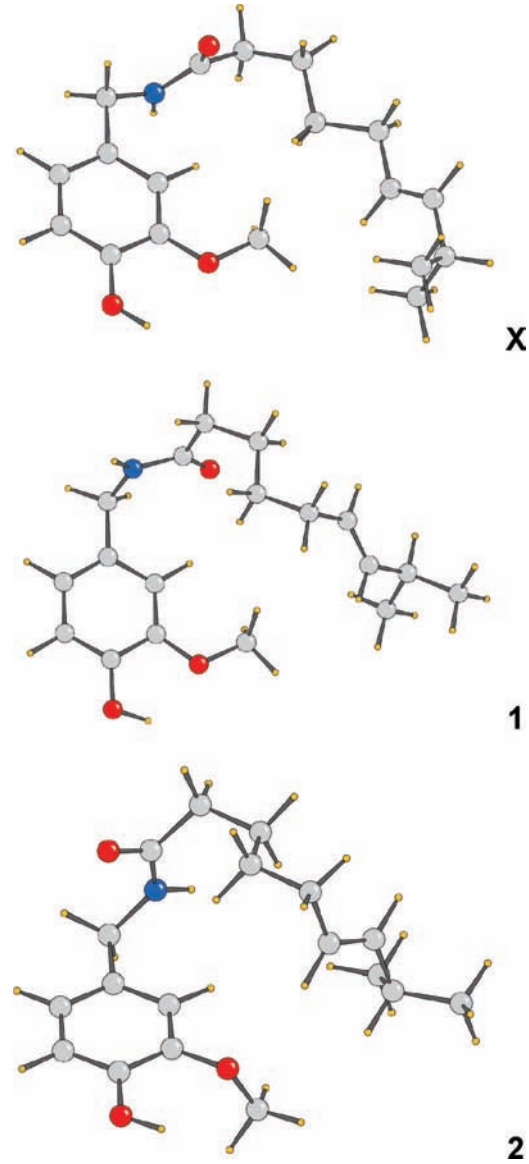

Figure 2. X-ray molecular structure of **CA** (top) and DFT-optimized geometries of its two lowest-energy conformers, **1** (middle) and **2** (bottom).

A common, distinctive structural feature of many conformers is the trans arrangement of both the H—N—C═O (amidic) and the H—C═C—H (ethenic) groups in the side chain. Another noteworthy point is the intramolecular hydrogen bonding

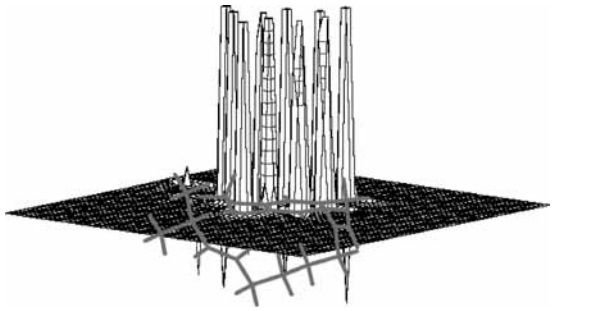

Figure 3. Laplacian plot of the **CA** structure (lowest-energy conformer).

between the two neighboring hydroxy and methoxy groups of the aromatic ring. As a further comment on the structure, it must be noted that the DFT values of the electric dipole moment, reported in Table 1, reflect significant differences in the overall distribution of charge in the various conformers.

The closeness of the computed conformer energies suggests the presence of a large number of them both in the gas phase and in a solvated environment, as well as low isomerization barriers. This conclusion is in agreement with the molecular dynamic simulations performed by Lambert and Sum[6] in an 1-octanol/water system. As a consequence of this energetic situation, the assignment of the various spectroscopic values to any of the calculated conformers is precluded. In principle, a proper consideration of the Boltzmann distribution of the various populations would be required. Yet, because of the size of the **CA** molecule and the multitude of conformers, this task would require an exceedingly large computational effort. Therefore, we must only consider a paradigmatic reference by restricting the comparison of the experimental data with the values calculated for the lowest-energy conformers **1** and **2**.

An interesting aspect of the electronic structure of **CA** is its Laplacian, that is, the second gradient of the charge density, that determines the regions of space wherein electronic charge is locally concentrated and depleted (Figure 3). Thus, the peaks in the Laplacian are regions of electron deficiency or electrophilic regions on the **CA** molecule. Figure 3 shows that **CA** can not only donate but also withdraw electronic charge mainly through its aromatic moiety. (In fact, **CA** can bind to either protonated or deprotonated channels.)[29] The characteristics of its Laplacian and lowest unoccupied MO (LUMO, Figure 4) suggest that the electronic charge received by **CA** from a protein or Aβ oligomer (i.e., the potential binding site) will be delocalized over the aromatic moiety.

Another important structure−activity parameter, which plays a primary role in reactions involving radical intermediates, is the homolytic bond dissociation energy (BDE). Thus, in order to elucidate the most favorable reaction site of **CA** for radical scavenging, the BDE for hydrogen abstraction from various molecular subunits, C_5—H phenyl, C_7—H benzylic, C_{13}—H olefinic, C_{15}—H methinic, O—H hydroxyl, and N—H amidic, was calculated for conformer **1** by optimizing the structures of the relevant radical species. Because the biological activity of **CA** occurs in solution, it would be very important to gain some information on its conformational preferences in a solvated environment. Unfortunately, the reoptimization of the gas-phase equilibrium structures at the DFT/MPWB1K level with the PCM model[21] in a polar solvent encountered a severe convergence difficulty. Thus, we only obtained the BDE values in the gas phase (C_7—H, 88.9; O—H, 91.0; N—H, 112.7; C_5—H, 119.3; C_{13}—H , 111.5; C_{15}—H, 85.5 kcal mol^{-1}).

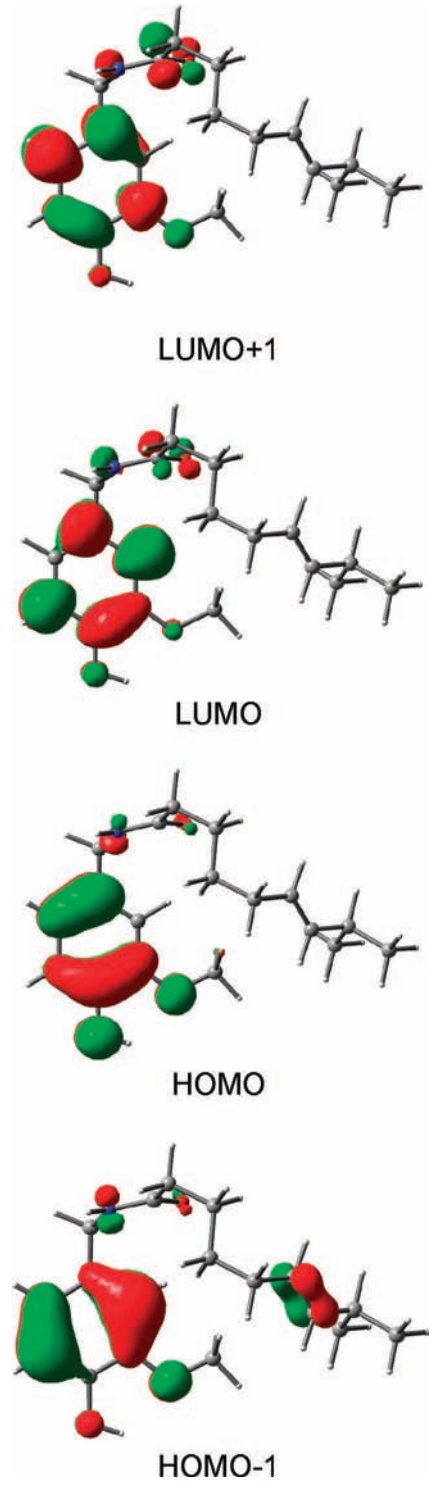

Figure 4. Frontier MOs of the lowest-energy conformer of **CA**.

Of the various radical intermediates, the (C_{15})-allyl and (C_7)-benzyl radicals turn out to be the more stable, likely because of a better stabilization by a resonance effect of the allyl and acetamide moieties. Then, the BDEs of the C_{15}—H and C_7—H subunits are the lowest, suggesting that the hydrogen-atom abstraction should mainly occur at these sites of the **CA** molecule. This DFT result corroborates the mechanism of oxidation of dihydrocapsaicin (**dhCA**, i.e., **CA** without the olefinic and methinic hydrogens) with DPPH radicals proposed by Nakamura et al.[30] Accordingly, in the first step of this process, the DPPH radical attacks the C_7 position of **dhCA**, forming a benzyl radical. Another DPPH radical abstracts the

TABLE 2: Observed and Calculated Vibrational Frequencies (cm^{-1})

	1		2	
obsd[a]	calcd	PED and assignment[b]	calcd	PED and assignment[b]
3696	3637	93 OH s	3636	90 OH s
3445	3463	99 NH s	3460	100 NH s
	3065	93 CH s (ring)	3065	99 CH s (ring)
	3056	98 CH s (ring)	3055	98 CH s (ring)
	3034	94 CH s (ring)	3036	100 CH s (ring)
	3019	98 CH s (OMe)	3019	95 CH s (OMe)
3016	2996	95 CH s (ethene)	2995	94 CH s (ethene)
1650	1677	69 C═O s (amide-I)	1681	72 C═O s (amide-I)
1629	1669	63 C═C s (ethene)	1667	61 C═C s (ethene)
	1660	58 CC s (ring)	1663	56 CC s (ring)
1598	1648	53 CC s (ring)	1649	48 CC s (ring)
1560	1564	26 CC s, 17 CO s, 22 HCC b (ring)	1569	18 CC s, 17 HCC b (ring)
1520	1528	35 HNC b, 34 CN s (amide-II)	1531	33 HNC b, 35 CN s (amide-II)
	1521	71 HCH b (Me)	1522	58 HCH b (Me)
	1505	75 HCH b (Me)	1505	67 HCH b (Me)
	1494	50 HCH b (Me)	1498	67 HCH b (Me)
1040	1077	56 OMe s	1075	48 OMe s
970	999	41 C═C t, 33 HC═C oop	973	34 C═C t, 33 HC═C oop

[a] Solid, ref 32. [b] PED in %; s = stretch, b = bend, t = torsion, oop = out-of-plane.

amidic hydrogen of the benzyl radical (BDE(N—H) 30.7 kcal mol^{-1}) leading to an amino-ketone, which tautomerizes to a methylene-quinone (ΔE = 8.4 kcal mol^{-1}). The C—N bond of this species is then hydrolytically cleaved by water.

Among the various spectroscopic observables of a compound, the ionization energies, electron attachment energies, and electronic transitions are the most direct manifestations of its electronic structure. However, also the vibrational frequencies are efficient monitors of the complex interplay of structural and electronic effects. Therefore, before discussing the main electronic properties of **CA**, it is worthwhile to briefly comment on its vibrational features.

The DFT calculations of the vibrational frequencies of **CA** were complemented with a normal coordinate analysis that provides the potential-energy distribution (PED in %) among the standard internal coordinates.[31] A selection of theoretical results for conformers **1** and **2** are reported in Table 2 together with the IR experimental values.[32] On the whole, the DFT reproduction of the observed frequencies is fair. It must be noted that the calculated vibrational pattern undergoes only minor changes on passing from **1** and **2**. The most characteristic vibrational features of the congested vibrational spectrum of **CA** are those of the amidic group and the two isolated absorptions at 1040 and 970 cm^{-1}. In particular, the bands observed at 1650 and 1520 cm^{-1} are associated with the amide-I band (C═O stretching vibration) and amide-II band (combination of NH bending and CN stretching vibrations), respectively. On the other hand, the 1040 cm^{-1} band is due to the OMe stretching. Interestingly, the 970 cm^{-1} band is specific of the trans double bond present in the side chain of the molecule; it arises from a combination of C═C torsion and CH out-of-plane vibrations. These last two prominent bands can be recognized as a distinctive fingerprint of **CA**.

Ionization Energies. Here, the experimental probing of the electronic structure of **CA** and **VN** through the analysis of the PE and electron-transmission (ET) spectra has been a fortiori extended to the fragment molecules **BA** and **MG**. Indeed, the low volatility of **CA** and **VN** at temperatures below 100 °C precluded to obtain a vapor pressure sufficient to record their ET spectra with our experimental setup. However, the spectroscopic results obtained for some reference molecules, complemented with suitable quantum-mechanical calculations, provide reliable background information to consistently characterize the electronic structure of **CA** and **VN**.

In order to advance a reliable interpretation of the PE spectra, reference is also made to the spectra of some small, related molecules, such as *trans*-4-methyl-2-pentene (**TMP**), *trans-N*-methyl-acetamide (**TMA**), and benzylamine (**BE**), that contain individual functional groups present in **CA**, **VN**, and their fragment molecules. Thus, for the $E_i(\pi_{C=C})$ of **TMP**, the experimental value[33] is 8.97 eV versus our OVGF value of 9.02 eV. For **TMA**, the experiment[34] yields E_is of 9.68 (π_N), 9.85 (n_O), and 12.5 ($\pi_{C=O}$) eV, and the OVGF predictions are 9.33, 10.07, and 12.68 eV, respectively. For **BE**, the OVGF results are 8.79 (π_A), 9.13 (π_S), 9.41 (π_N), and 11.94 (σ) eV, where π_A and π_S designate the antisymmetric and symmetric components of the benzene e_{1g} HOMO, respectively, and the experimental values are 8.96, 9.6, and 11.6 eV.[35] Therefore, the correspondence between experiment and OVGF theory for the $\pi_{C=C}$, $\pi_{C=O}$, π_N, n_O, and the uppermost phenyl $\pi_{S,A}$ E_is of these reference molecules is very satisfactory.

On this preliminary ground, the ab initio OVGF results reported in Table 3 yield a consistent description for the general features observed in the PE spectra of the compounds investigated (Figure 5). The pole strengths calculated for all investigated photoionization processes are larger than 0.85, which excludes the presence of nearby shakeup lines and thus indicates that the one-particle model of ionization is essentially correct.[36–38]

For both **BA** and **MG**, the lowest two PE bands, which fall in the 8—10 eV region, can be attributed to ejection of an electron from either of the two $\pi_{S,A}$ MOs of the benzene moiety of these molecules. As expected, the cumulative mesomeric and inductive effects of the hydroxy and methoxy groups in **MG** cause a marked shift of the highest occupied MO (HOMO) to higher energy relative to **BA**, with a consequent net splitting between the first two aromatic π E_is. Notably, the electron removal from the π_N MO of **BA** gives rise to a feature overlapped with the second band. Furthermore, the shoulder at 9.9 eV can be attributed to the n_O of the carbonyl group. The third band (peaked at 10.8 eV) displayed in the PE spectrum of **MG** is assigned to a MO composed of oxygen lone pairs (π_O) mixed with an aromatic π orbital.

VN is structurally analogous to **CA**, differing only by the lack of the lateral $\pi_{C=C}$ bond and one terminal methyl group.

TABLE 3: Vertical Ionization Energies (eV) and Assignment

$E_{i,expt}$	assignment	$E_{i,calcd}$
	BA	
9.0	π_S	8.74
9.5	π_A	8.98
	π_N	9.34
9.9 sh	n_O	10.18
11.75	σ	11.84
	MG	
8.05	π_S	7.66
8.85	π_A	8.63
10.8	π	11.02
11.5	σ	11.83
	VN	
8.0	π	7.76
9.2	π	8.75
9.4	π_N	9.12
	n_O	9.74
10.45	σ	10.67

$E_{i,expt}$	assignment	$E_{i,calcd}$, **1**	$E_{i,calcd}$, **2**
	CA		
8.2	π	7.72	8.01
8.9 sh	π	8.58	8.77
9.1	$\pi_{C=C}$	9.04	8.80
	π_N	9.22	9.25
9.7 sh	n_O	10.00	9.62
10.8	σ	11.00	10.76
	σ	11.22	10.97

This explains why the two compounds show largely similar PE spectra (Figure 5). Thus, the first band is generated by photoionization from the top π(methoxyphenolic) MO, and the second

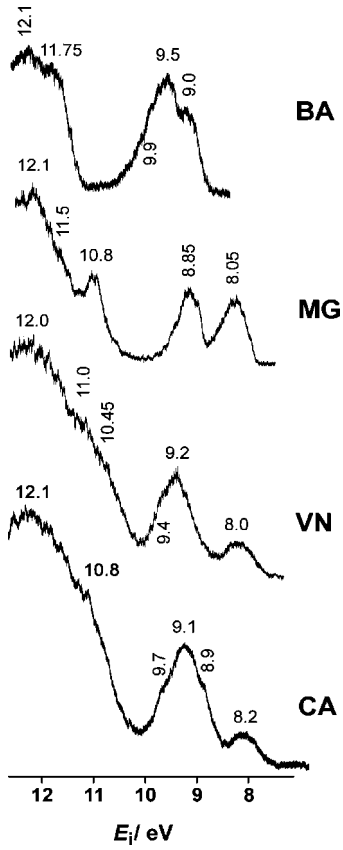

Figure 5. He(I) PE spectra.

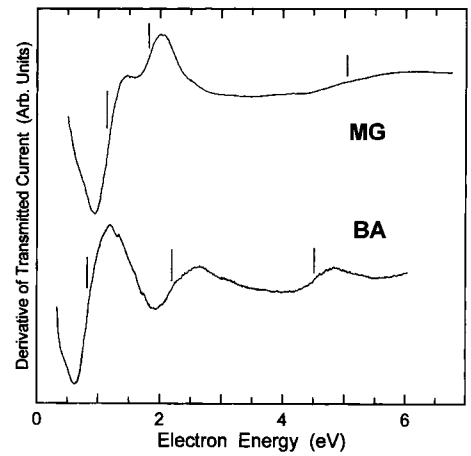

Figure 6. Derivative of transmitted current as a function of electron energy, in **MG** and **BA**. Vertical lines locate the VAEs.

broad band arises from various closely lying photoionizations, associated with another outermost π(methoxyphenolic) MO and the π_N, n_O, and $\pi_{C=C}$ MOs (the last only in **CA**). The prominent band system with onset at about 10 eV encompasses a congested manifold of σ and π photoionizations. Compared with **MG**, the position of the two outermost π MOs of **CA** (Figure 4) and **VN**, as well as their splitting, remain nearly unchanged, thereby indicating the modest electronic influence exerted by the long side chain on the filled frontier MOs.

As can be seen from the OVGF results reported in Table 3, the conformational change of **CA** is accompanied by a sizable but not monotonic displacement of the low-energy photoionizations. The same behavior applies also to **VN**. Therefore, owing to the marked flexibility of the side chain in the **CA** an **VN** molecules, the presence of several conformers in the gas phase could partially account for the broad, unresolved structure of the second band in their PE spectra.

Electron Attachment Energies. Figure 6 reports the ET spectra of **MG** and **BA**. The measured vertical electron attachment energies (VAEs) are given in Table 4.

A theoretical approach adequate for describing the energetics and nature of anion states involves difficulties not encountered for neutral or cation states.[39] The first VAE can, in principle, be calculated as the energy difference between the lowest-lying anion and the neutral state (both with the geometry of the neutral species). A proper description of the spatially spread electron distribution of unstable anions requires a basis set with diffuse functions.[40] However, as the basis set is expanded, a self-consistent field calculation ultimately describes a neutral molecule and an unbound electron in as much of the continuum as the basis set can emulate. These low-energy solutions have no physical significance with regard to anion formation,[41–45] and stabilization procedures are then needed to distinguish them from the virtual orbitals that give rise to temporary anion states.[43–45] In addition, the dependence of the calculated energies on the addition of diffuse functions to the basis set increases with increasing anion-state instability.[46]

However, it has been shown[41,42,47] that simple Koopmans's theorem calculations (with basis sets without diffuse functions), using empirical linear scalings of the corresponding VOEs, can satisfactorily reproduce the π^* VAEs measured in a large number of π systems. Here, this simple and reliable procedure is used to support the association of the resonances observed in the ET spectra of **MG** and **BA** with the corresponding empty π^* MOs (systematic ETS studies have in fact shown that empty σ^* MOs give rise to distinct low-energy features only in the

TABLE 4: Virtual Orbital Energies (VOEs) Supplied by B3LYP/6-31G(d) Calculations and Experimental VAEs[a]

orbital	VOE	scaled VOE	expt VAE
	Benzene[b]		
π^*b_{2g}	4.461	4.67	4.82
π^*e_{2u}	0.099	1.19	1.12
	MG		
π^*_O	4.569	4.76	5.1
π^*_S	0.579	1.57	1.81
π^*_A	0.383	1.41	1.17
	BA		
π^*_O	4.136	4.41	4.5
π^*_{CO}-n_N	0.888	1.82	2.20
π^*_A	0.033	1.14	
π^*_S	−0.128	1.01	0.85
	VN		
π^*_O	4.416	4.64	
π^*_{CO}-n_N	0.876	1.81	
π^*_S	0.216	1.28	
π^*_A	0.125	1.21	
	CA		
π^*_O	4.305	4.55	
π^*_{CO}-n_N	0.878	1.81	
π^*_{CC}	0.686	1.66	
π^*_S	0.438	1.46	
π^*_A	0.151	1.23	

[a] All values in eV. Scaled VOEs (see text) in parentheses. [b] VAEs from ref 26.

ET spectra of compounds containing third row or heavier elements).[48] Most importantly, the scaled VOEs allow a quantitative prediction of the π^* VAEs of **VN** and **CA**, the ET spectra of which were not recorded because a sufficiently high vapor pressure could not be obtained under our experimental conditions.

In order to employ an accurate empirical scaling, directly biased toward the π-groups which constitute **CA**, we have used a relationship derived[49] only from the VAEs of dehydrozingerone (where, at variance with **CA**, the *o*-methoxyphenol, ethene, and carbonyl π functionals are conjugated) and smaller reference molecules. This equation (VAE = 0.7985 VOE + 1.1098, $r^2 = 0.987$) is close to that previously obtained[47] from a large number of π^* VAEs and the corresponding B3LYP/6-31G(d) VOEs.

The B3LYP/6-31G(d) π^* VOEs of the neutral state molecules benzene, **MG**, **BA**, **VN**, and **CA** are given in Table 4 together with the corresponding scaled values. The geometries of **BA**, **VN**, and **CA** were recalculated from the preferred conformers obtained at the DFT/MPWB1K/6-31+G(d,p) level.

The experimental VAEs of benzene[26] are closely reproduced by the corresponding scaled VOEs, the VAEs of the degenerate e_{2u} (π^*) LUMO and of the higher-lying totally antibonding b_{2g} (π^*) MO being slightly over- and under-estimated, respectively. In **MG**, interaction with the oxygen lone pairs[48] removes the degeneracy of the benzene e_{2u} (π^*) LUMO. Its two components π^*_S and π^*_A give rise to the resonances located at 1.17 and 1.81 eV, respectively, in the ET spectrum. The energy splitting predicted by the calculations is underestimated (see Table 4) although, because of partial overlap between the two resonances and the smaller intensity of the second one, the measured value of 1.81 eV is to be considered an upper limit of the second VAE. The third resonance, centered at 5.1 eV, is associated with the empty MO (here denoted as π^*_O) deriving from the benzene b_{2g} (π^*) MO, destabilized by mixing with the oxygen lone pairs. However, its width (about 1.7 eV) is much larger than that of the corresponding resonance in the spectra of benzene and **BA**, indicating that this feature must comprise an additional unresolved contribution from a higher-lying core-excited resonance, that is, electron capture into the LUMO accompanied by HOMO → LUMO excitation. In agreement, this core-excited state is expected to lie at lower energy than in benzene (where it is located at about 6.0 eV)[50] because of the large destabilization of the π HOMO due to mixing with the oxygen lone pairs.

In **BA**, the carbonyl group introduces an additional empty π^*_{CO} MO, mixed with the adjacent nitrogen lone pair orbital n_N. This destabilizing interaction increases the VAE (about 1.3 eV in acetone and cyclic ketones) of the π^*_{CO} MO by about 1 eV.[51] Consistently, the ET spectrum of **BA** displays a resonance at 2.20 eV ascribed to electron attachment to the π^*_{CO} MO. The intermediate CH_2 group prevents conjugation between the N−C═O and benzene π fragments. Because of the small energy perturbations caused by alkyl groups on adjacent π^* MOs,[48] the anion states formed by occupation of the three benzene π^* MOs are expected to be mainly affected by the electron withdrawing effect of the carbonyl group. In agreement, these anion states are about 0.3 eV more stable than in benzene and, as predicted by the calculations, the π^*_S and π^*_A VAEs are so close to each other that their contributions to the first resonance of the ET spectrum are not resolved.

The reliability of the scaled VOEs in reproducing the VAEs measured in the smaller reference molecules gives confidence that the same approach is also suitable for evaluating the energies of the vertical anion states of **VN** and **CA**. The empty-level structure of **VN** is similar to that of **BA**. However, the presence of the OH and OCH_3 substituents in **VN** is expected to destabilize the ring π^* anion states (mainly π^*_S), and the eight-member alkyl chain on the carbonyl group should reduce its electron-withdrawing effect toward the benzene ring. The first scaled VOE (1.21 eV) of **VN**, associated with the π^*_A MO, is essentially equal to that of benzene. Instead, the predicted π^*_S VAE (1.28 eV) is likely underestimated by about 0.2 eV, as observed in **MG**. Finally, the scaled π^*_{CO} VOE is the same as that of **BA**, where the experimental VAE is 2.20 eV.

Although the alkyl chain attached to the carbonyl group is saturated in **VN**, in **CA**, a single C−C bond is replaced with a nonconjugated double C═C bond, bearing an additional empty π^*_{CC} MO. The π^*_{CC} VAE of *trans*-2-butene (where the ethene functional is dialkyl substituted as in **CA**) is 2.10 eV.[52] Once the inductive effect of the carbonyl group is accounted for, the π_{CC}* VAE of **CA** is expected to be close to that (1.73 eV)[26] of ethene, in good agreement with the scaled VOE (1.66 eV, Table 4). The calculations predict the π^*_{CO} anion state of **CA** to lie at the same energy as that in **VN** and **BA**. The scaled VOE 1.23 eV of the π^*_A LUMO of **CA** is very close to those of **VN** (1.21 eV) and benzene (1.19 eV). The experimental VAE of benzene is 1.12 eV,[26] so that a negative vertical electron affinity of about −1.2 eV can be estimated for **CA**.

Thus, although **CA** contains the same π functionals as dehydrozingerone (also referred to as half-curcumin), its electron-acceptor properties are quite smaller. In the latter system, the *o*-methoxyphenol, ethene, and carbonyl π-fragments are adjacent to each other and form a strongly conjugated π system with a positive electron affinity of about 0.2 eV,[49] whereas both the energy and localization properties of the first anion state of **CA** (the LUMO of which is depicted in Figure 4) are close to those of benzene.

Electronic Transitions. Two bands are observed in the UV spectrum of CA in ethanol solution,[53,54] that is, the secondary

TABLE 5: Electronic Transitions: Energies (nm) and Intensities (Oscillator Strength *f*, Molar Absorptivity ε), Calculated Values for Conformers 1 and 2

expt	calcd			calcd		
λ (ε)	λ	*f*	composition of wave function[b]	λ	*f*	composition of wave function
CA[a]			1			2
280 (2800)	250	0.073	0.60 (H→L) + 0.24 (H−1→L+1)	250	0.068	0.61 (H→L) − 0.26 (H−1→L+1)
227 (8100)	225	0.157	0.57 (H→L+1) − 0.23 (H−1→L)	233	0.103	0.63 (H→L+1) − 0.14 (H→L+3)
	216	0.011	0.38 (H−3→L) + 0.33 (H−3→L+3)	223	0.004	0.70 (H→L+2)
	212	0.002	0.69 (H→L+2)	218	0.008	0.40 (H−3→L+1) − 0.36 (H−3→L+3)
	208	0.003	0.59 (H→L+3) + 0.29 (H−3→L)	209	0.017	0.62 (H→L+3) + 0.19 (H−3→L+1)
	206	0.027	0.34 (H−1→L) − 0.34 (H−3→L)	206	0.002	0.54 (H−2→L) + 0.44 (H−1→L)
	203	0.002	0.59 (H−2→L) + 0.31 (H−1→L)	204	0.002	0.52 (H−2→L+1) + 0.45 (H−1→L+1)
	198	0.077	0.33 (H−1→L+1) − 0.32 (H−3→L+1)	201	0.015	0.61 (H−3→L) + 0.22 (H→L+4)
	195	0.100	0.33 (H−4→L+1) − 0.30 (H−3→L+1)	200	0.002	0.64 (H→L+4) − 0.19 (H−3→L)
	193	0.090	0.38 (H−4→L) − 0.33 (H−1→L+1)	199	0.099	0.42 (H−3→L+1) + 0.38 (H−4→L+1)
Ca$^-$			**1**(O$^-$)			**2**(O$^-$)
	304	0.001	0.70 (H→L)	297	0.045	0.60 (H→L) − 0.26 (H→L+1)
295 (4300)[c]	291	0.087	0.67 (H→L+1)	291	0.044	0.52 (H→L+2) − 0.35 (H→L+1)
	279	0.096	0.63 (H→L+2) + 0.14 (H→L+4)	287	0.056	0.54 (H→L+1) + 0.41 (H→L+2)
	262	0.006	0.65 (H→L+3) + 0.23 (H→L+4)	263	0.001	0.64 (H-1→L) − 0.25 (H-1→L+2)
	248	0.000	0.65 (H−1→L+2) − 0.17 (H−1→L+4)	250	0.022	0.44 (H→L+4) - 0.29 (H-1→L+1)
252 (11000)	244	0.240	0.59 (H→L+4) − 0.19 (H→L+3)	248	0.015	0.46 (H→L+4) + 0.33 (H-1→L+1)
	239	0.000	0.57 (H−1→L+1) + 0.36 (H−1→L+4)	241	0.133	0.54 (H→L+3) − 0.28 (H→L+4)
	233	0.007	0.65 (H→L+5) − 0.20 (H→L+7)	238	0.002	0.56 (H-1→L+2)- 0.37 (H−1→L+1)
	231	0.000	0.70 (H−1→L)	227	0.002	0.48 (H→L+7) + 0.48 (H→L+6)
224 (6700)	229	0.006	0.64 (H→L+6) − 0.18 (H→L+8)	224	0.008	0.64 (H→L+5) + 0.22 (H→L+7)
	222	0.005	0.66 (H→L+7) + 0.21 (H→L+5)	222	0.001	0.51 (H−1→L+3) − 0.39 (H−1→L+1)

[a] In ethanol solution at pH = 7.4, ref 53. [b] Principal electronic configurations; H and L stand for HOMO and LUMO, respectively. [c] In ethanol solution at pH = 12.8, ref 53.

band at 280 nm (the ^1L_b band in Platt's notation for benzenoid compounds) and the primary band at 227 nm (the ^1L_a band). Both bands have a rather small intensity (ε = 2800 and 8100, respectively) and arise from $\pi \rightarrow \pi^*$ transitions. TD-DFT calculations indicate that they partially resemble those of phenol (observed at 269 and 210 nm).[55] Indeed, conjugation of the oxygen lone pair of the methoxy group and the π network of the amidic group with the aromatic π system leads to a red-shift of both bands.

To illustrate the electronic excitations, the frontier MOs of the preferred conformer **1** are shown in Figure 4. All of these MOs are of essential π character. The π network is concentrated over the guaiacol moiety in the HOMO, whereas it also involves the ethenic unit in the HOMO − 1. On the other hand, the π network also propagates into the amidic unit in the LUMO and LUMO + 1.

In the present calculations, the solvent (ethanol) effect was taken into account with the PCM formalism.[21] The TD-DFT results for conformers **1** and **2** are gathered in Table 5 together with the experimental results. In this respect, it is worthwhile to mention that previous reports place transition energies given by TD-DFT within approximately 0.3 eV of experimental values.[19,56,57] According to the TD-DFT results, the lowest-energy band of **CA** at 280 nm is associated with the first predicted electronic transition, the major component of which is the HOMO → LUMO excitation. The HOMO → LUMO + 1 excitation is instead the principal contributor to the primary band at 227 nm. As for the structural effects, shown by conformers **1** and **2**, the excitation energies of **CA** are slightly sensitive to conformational change.

In a strongly basic medium, **CA** undergoes deprotonation from the phenolic group, and the absorption spectrum of the resulting closed-shell anionic species **Ca**$^-$ exhibits a bathochromic shift associated with a hyperchromic effect and the appearance of a third band.[53] Notably, the most intense transitions of the ionized species **Ca**$^-$ have a composition quite different from that of the parent neutral compound **CA** (Table 5). Thus, the HOMO → LUMO excitation of **Ca**$^-$ gives rise to a very weak feature hidden under the band at 295 nm. Indeed, the lowest-energy absorption of **Ca**$^-$ is mainly due to the excitations HOMO → LUMO + 1 and HOMO → LUMO + 2. Furthermore, the prominent band of **Ca**$^-$ centered at 252 nm corresponds to the HOMO → LUMO + 4 excitation. Various electron promotions from the HOMO to higher unfilled MOs cause absorption at around 224 nm. It is important to remark that Kogure et al.,[53] from the relatively modest bathochromic displacement observed in the absorption spectrum on passing from **CA** to **Ca**$^-$, argued that the phenolic OH group remains intact after reaction of **CA** with DPPH radicals in alkaline solution. This conclusion is corroborated by the present TD-DFT results for the phenoxyl neutral (open-shell) radical **Ca•**. Accordingly, the conversion of **CA** to **Ca**$^-$ should be accompanied by a large bathochromic shift and the evident change from colorless to red, as a consequence of a sizable absorption predicted for the phenoxyl radical in the visible region (λ = 416 nm, f = 0.027; λ = 454 nm, f = 0.004; and λ = 593 nm, f = 0.015).

ESR Measurements. Efforts were made to generate the radical anions of **CA** and **VN** and to characterize them by means of ESR spectroscopy. Several different techniques were used, and in all experiments, **CA** and **VN** exhibited the same reactivity leading to identical ESR spectra under the same reaction conditions. Therefore, only the reduction of **CA** will be dealt with in the following.

Although in nearly all the experiments, intense ESR signals were detected, in no case could the observed spectra be attributed to radical anions of the original compound. In order to attempt a reasonable identification of the various reduction products of **CA**, several radical models were taken into account. A selection is shown in Figure 7, and the relevant isotropic HFCCs

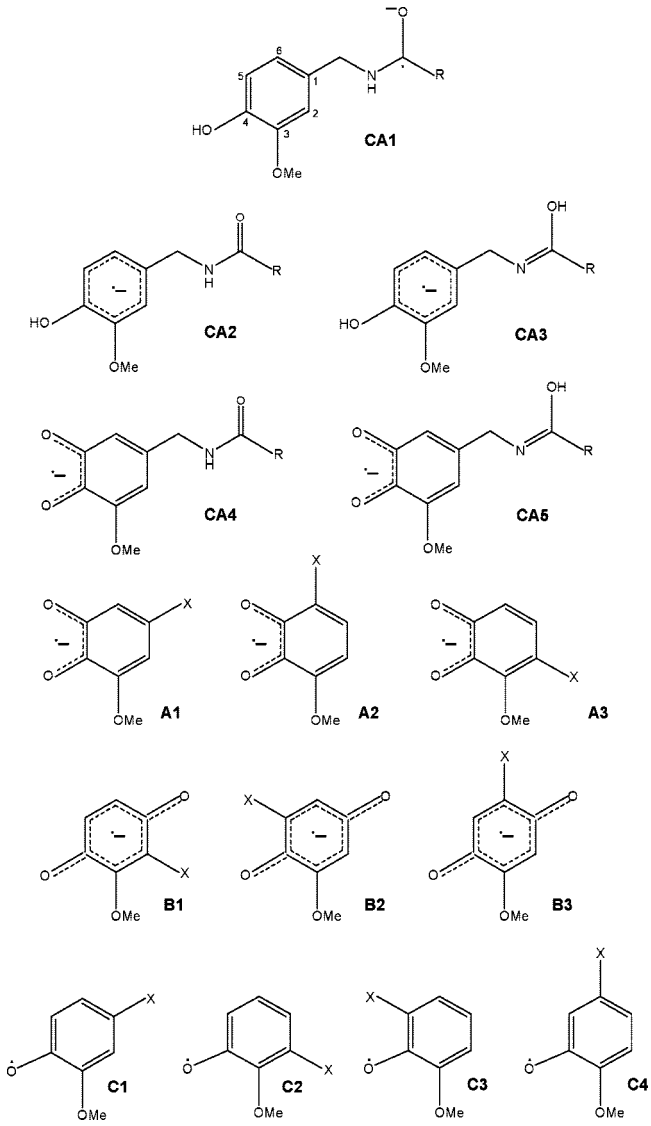

Figure 7. Model radicals for the **CA** reduction process. X represents an ESR-inactive substituent.

calculated with the DFT/B3LYP/PCM/EPR-II formalism are presented in Table 6. In this connection, it must be recalled that the accurate reproduction of ESR data for complex organic radicals by quantum-mechanical calculations, even at the highest available theoretical level, is still a challenging task because they are strongly dependent on electron correlation, basis set, and solvent effects.[58–60] However, a fair reproduction of the HFCCs of the related simple systems, 3-methoxy-1,2-benzosemiquinone radical anion (exp. $a_{Me} = 0.060$, $a_{H4} = 0.160$, $a_{H5} = 0.400$, $a_{H6} = 0.018$ mT;[61] calcd. 0.095, −0.109, −0.371, −0.024 mT), 2-methoxy-1,4-benzosemiquinone radical anion (exp. $a_{Me} = 0.08$, $a_{H3} = -0.059$, $a_{H5} = -0.364$, $a_{H6} = -0.204$ mT;[62] calcd. 0.079, −0.080, −0.368, −0.212 mT), and phenoxyl radical of guaiacol (exp. $a_{Me} = 0.18$, $a_{H3} = 0.18$, $a_{H4} = 0.83$, a_{H5} = unresolved, $a_{H6} = 0.42$ mT;[63] calcd. 0.214, 0.239, −0.835, 0.104, −0.510 mT) lends some confidence to the present DFT predictions (Table 6).

The reduction of **CA** was first attempted by reaction with potassium *tert*-butoxide in DMSO. This led to the observation of the spectrum of radical **R1** shown in Figure 8, which indicates coupling of the unpaired electron with three equivalent hydrogen atoms (a methoxy group) and two different hydrogen atoms. The spectral parameters (Table 7) are inconsistent with the radical **CA1** resulting from reduction of the carbamic group of **CA**, for which a relatively large triplet splitting of the α methylenic group along with a nitrogen splitting is expected. They do not seem appropriate also for the radical anion of a 4-substituted *ortho*-methoxy-phenol (structures **CA2** and **CA3**) resulting from reduction of the aromatic moiety. Indeed, the g value is higher than expected ($g \leq 2.0040$) when considering that a vanishingly small spin density is predicted at the oxygen atoms, and the HFCCs for the ring hydrogen atoms are much smaller than the calculated values.

The measured spectral parameters fit reasonably with those of substituted 3-methoxy-1,2-semiquinones.[64–66] In this case, a nucleophilic attack of water (possibly traces of humidity in the solvent) on the phenolic moiety might lead to the formation of an *ortho*-hydroquinone which would eventually autoxidise to a semiquinone in the basic medium. Yet, as shown in Table 6, disubstituted *ortho*-semiquinonic systems such as **CA4** or **CA5** would require a detectable triplet splitting from the two hydrogen atoms of the methylenic group bound to the aromatic ring. On the other hand, if the loss of the side chain is assumed (structures **A1**−**B3**), a better agreement between the experimental and computed HFCCs is obtained, the best fit being provided by structures **A2**, **B1**, or **B2**.

As time goes by, the spectrum starts to evolve and is eventually replaced by another one where the signals from at least two species are superimposed, both indicating the interaction of the unpaired electron with a methoxy group. No attempts were however made to identify these radicals that may originate from further evolution of semiquinones **A1**−**B3**. In any case, both the nature of X (a *tert*-butoxyl group?) and the way in which species **A1**−**B3** may be formed remain to be clarified.

The in situ electrolytic reduction of **CA** in DMSO by using Bu_4NClO_4 as supporting electrolyte also led to observation of several ESR spectra. Figure 9a shows the spectrum initially detected at the lowest potential leading to observation of an ESR signal. The spectrum originates from the superimposition of the signals from three radical species present in similar amounts. The first (radical **R2**) exhibits a weak coupling of the unpaired electron with three magnetically different hydrogen atoms. The unpaired electron interacts with three hydrogen atoms also in radical **R3**, although more intensely than in **R2**, whereas species **R4** shows coupling of the unpaired electron with two hydrogen atoms and a methoxy group. The lack of the methoxy splitting and the very small values of the other HCCs exhibited by **R2** are not in line with either the radical anion of the original compound (**CA1**, **CA2**, or **CA3**) or with a quinonic structure like **CA4**−**CA5**, **A1**−**A3**, or **B1**−**B3**, and we have no sensible suggestion about its structure.

Although the spectrum of species **R4** is somehow reminiscent of that observed for radical **R1** and might therefore be attributed to a semiquinone like **A1**−**A3** or **B1**−**B3**, it is hard to hypothesize the structure of radical **R3**. Indeed, the lack of a splitting from the methoxy group leads to exclude, beside structures **A1**−**A3** or **B1**−**B3**, also a 6-substituted-2-methoxy-phenoxyl radical (structure **C3**), as both calculations (Table 6) and literature data[67] indicate that the hydrogen atom H-1 should have a substantial splitting ($a_{H1} \geq 0.8$ mT) and also the HFCC of the methoxy group should be fairly large ($a_{3H} \approx 0.2$ mT). Following the first small potential increase, the central signal due to radical **R2** vanishes, and only those due to species **R3** and **R4** remain detectable (Figure 9b). Upon further increase of the potential, a decrease of the intensity of the signal due to species **R3** is also observed (Figure 9c), and eventually, only the spectrum of **R4** remains detectable. Actually, this radical

TABLE 6: DFT Calculated Values of the Isotropic HFCCs (mT) of Selected Radical Models in DMSO Solution

radical[a]	H-1[b]	H-2	CH_3	H-5	H-6	CH_2	^{14}N
CA1,**CA2**		−0.691	0.033	−0.575	0.104	0.276	0.570
CA3		−0.638	0.017	−0.505	0.095	0.460	0.286
CA4		−0.098	0.066		−0.088	0.129	0.156
CA5		−0.136	0.094		−0.062	0.154	0.080
A1	X	−0.124	0.101		0.024		
A2	−0.322	−0.140	0.085		X		
A3	−0.409	X	0.071		−0.020		
B1		X	0.067	−0.251	−0.372		
B2		−0.101	0.079	X	−0.310		
B3		−0.078	0.083	−0.151	X		
C1	X	0.234	0.202	−0.469	0.053		
C2	−0.792	X	0.259	−0.479	0.092		
C3	−0.826	0.241	0.198	X	0.164		
C4	−0.876	0.241	0.225	−0.416	X		

[a] In the calculations, the X substituent of radicals **A1**−**C4** was treated as a single methyl group. The **CA** radicals were modeled from the lowest-energy conformer. [b] For atom numbering, see Figure 7.

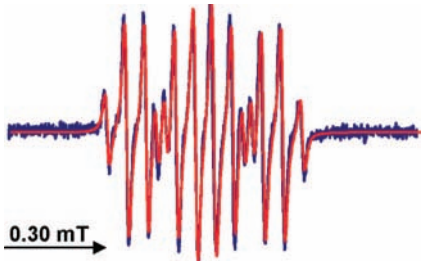

Figure 8. ESR spectrum observed at room temperature upon reaction of **CA** with potassium *tert*-butoxide in DMSO (blue line) and its computer simulation (red line).

seems fairly persistent, as it may be expected for a semiquinone radical anion, and its clean spectrum (Figure 9d) can be observed for several minutes after the applied potential has been switched off. Among species **A1**−**A3** and **B1**−**B3**, radical **A3** appears to be the one providing the best agreement between calculated ESR spectral parameters and those experimentally determined for radical **R4**.

It is well established that alkali metal reduction of either carbonyl compounds or aromatic hydrocarbons readily affords the corresponding radical anions. Nevertheless, contrary to expectation, when thoroughly degassed THF solutions of either **CA** or **VN** were put in contact with a sodium metal mirror inside the cavity of the ESR spectrometer in a temperature interval ranging from 193 to 298 K, no signal was detected. Also, attempts to stabilize the possibly formed radical ion pairs through complexation of the alkali metal counterion failed. Thus, no apparent reaction was observed even in the presence of dibenzo-18-crown-6-ether, an additive known to be an excellent complexing agent for sodium cation.

At variance, the photoassisted reaction of **CA** or **VN** with sodium ethoxide in ethanol/dimethoxyethane 1:1 led to the observation of a spectrum consisting of the superimposition of at least two main signals (Figure 10), the simulation of which is not very satisfactory because of the presence of additional signals from other minor species. The spectral parameters used in the simulation are collected in Table 7 (entries **R5** and **R6**). Once again, radical **R5** exhibits HFCCs in line with a substituted semiquinone, and structures **A2**, **B1**, and **B2** are those that show a more reasonable agreement between experimental and calculated values. More interestingly, the spectral parameters of radical **R6** indicate that the unpaired electron also interacts with a nitrogen and two equivalent hydrogen atoms. Structures **CA2** and **CA3** do not justify the relatively large *g* value. Thus, we identify radical **R6** as species **CA5**, because **CA4** is less likely due to the absence of a splitting from the NH hydrogen atom. Actually, position 1 should be characterized by a relatively high spin density, and a value of 0.258 mT for the methylenic splitting appears reasonable. As for the nitrogen, the value of its coupling may reflect efficient hyperconjugation due to a favorable conformational preference.

In order to exclude the occurrence of artifacts due to UV−vis irradiation of **CA** (**VN**), photolysis of these compounds was also carried out in benzene solution in the presence of a small amount of 2-methyl-2-nitrosopropane as spin trap. The only spectrum observed belonged to di*tert*-butyl-peroxide and, as expected, faded away upon prolonged irradiation, whereas no ESR evidence of formation of an acyl-nitroxide, originating from a photoinduced cleavage of the $-CH_2-C(O)-$ bond, was obtained.

Finally, both **CA** and **VN** were allowed to react with the superoxide radical anion generated in DMSO solution as described in the literature.[68] Once again, a strong spectrum identical to that shown in Figure 8 and attributed to species **A2**, **B1**, or **B2**, was detected. We believe this to be a fairly surprising finding, because although electron transfer from a quinone or quinoneimine radical anion to oxygen to give the superoxide radical anion is well documented,[69,70] the reverse process should be hampered by adverse redox potentials.

Overall, the ESR experiments indicate that **CA** is generally unstable toward reduction, a process that seems to involve the aromatic moiety, being rapidly converted to a quinonic derivative. In most cases, **CA** also undergoes molecular degradation, likely through cleavage of the bond between the aromatic moiety and the aliphatic chain.

Concluding Remarks

The conformational preferences of **CA**, a pharmacophore currently employed to trigger a number of physiological effects, have been studied by using the hybrid meta DFT method MPWB1K of Zhao and Truhlar[11] in combination with the 6-31+G(d,p) basis set. Owing to the marked flexibility of the pendant side chain, **CA** can adopt a multitude of conformations, slightly different in energy. However, consideration of the lowest two conformers allows for a reliable structural and electronic characterization of the compound investigated. Thus, according to the calculated bond dissociation energies, the most favorable reaction sites of **CA** for radical scavenging are the C_{15}-allyl and C_7-benzyl carbons. A study of the filled and empty electronic structure of **CA** has been carried out by taking

TABLE 7: ESR Spectral Parameters (HFCCs in mT) for the Radical Species Observed upon Reduction of either CA or VN under Different Conditions

radical	solvent and reduction process	*a*(**3H**)	*a*(**1H**)	*a*(**1H**)	*a*(**1H**)	*a*(**2H**)	*a*(**1N**)	*g*	possible structure
R1	DMSO/^{t}BuOK DMSO/KO_2/CE[a]	0.060	0.152	0.265				2.0050_0	**A2**,**B1**,**B2**[b]
R2	DMSO electrol.		0.023	0.059	0.081			2.0047_7	**?**[c]
R3	DMSO electrol.		0.053	0.167	0.554			2.0047_3	**C3?**[d]
R4	DMSO electrol.	0.052	0.030	0.372				2.0048_2	**A3**[b]
R5	EtOH/DME EtONa	0.088	0.195	0.453				2.0045_5	**A2**,**B1**,**B2**[b]
R6	EtOH/DME EtONa	0.073	0.103	0.278		0.258	0.234	2.0045_5	**CA5**[e]

[a] CE = dibenzo-18-crown-6-ether. [b] Structures **CA3** and **CA4** seem unlikely due to lack of a CH_2 splitting. [c] **CA1** and **CA2** are ruled out by DFT prediction of a large spin density on the ring. [d] Very questionable, because the OCH_3 splitting should be fairly large (ca. 0.15−0.2 mT). [e] Assignment based on detection of a ^{14}N splitting and lack of H(NH) splitting.

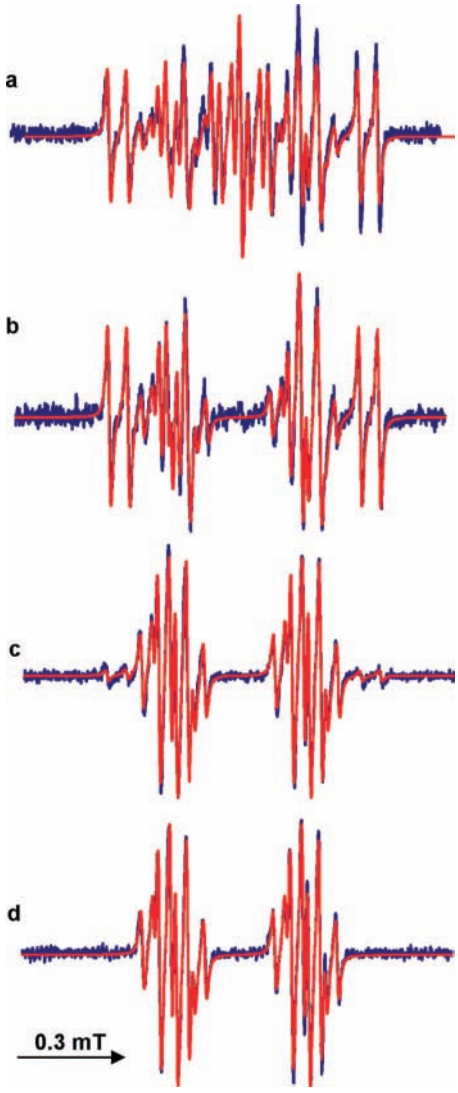

Figure 9. ESR spectra observed at room temperature upon electrochemical reduction of **CA** in DMSO containing Bu_4NClO_4 (blue lines) at lower (a) and higher (d) applied potentials and their computer simulations (red lines).

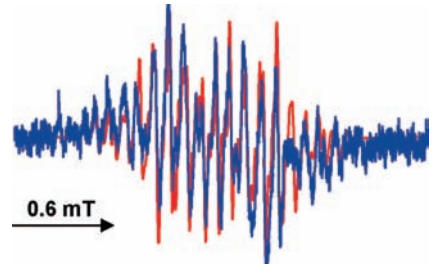

Figure 10. ESR spectrum observed at room temperature upon reduction of **CA** with EtONa in EtOH/DME 1:1 v/v (blue line) and its computer simulation (red lines).

advantage of the PE and ET spectra also obtained for related fragment molecules and suitable quantum-mechanical (ab initio OVGF and DFT) calculations. Thus, detailed assignments of the low-energy photoionization and electron attachment processes of **CA** have been proposed. In the π-frontier MOs of **CA**, only a modest interaction between the vanillyl moiety and the amidic-aliphatic chain is operative. The low-lying electronic excited states of **CA** have been characterized in terms of the main one-electron jumps. The TD-DFT calculations have also provided a consistent picture of the spectroscopic change observed by deprotonation of the phenolic group of **CA** in alkaline ethanolic solution (modest bathochromic shift and appearance of a new absorption band) and expected upon conversion of **CA** into a phenoxyl neutral radical (colorless to red).

ESR experiments indicated that **CA** quickly undergoes fragmentation upon reduction. As a consequence, although the corresponding radical anion could not be observed, a variety of radicals were instead detected, the more persistent of which were assigned a semiquinonic structure.

Acknowledgment. V.G. and A.M. thank the Italian Ministero dell'Istruzione, dell'Università e della Ricerca. B.K. thanks the Ministry of Science, Education and Sports of the Republic of Croatia through Project 098-0982915-2945 for support of this work. F.P. thanks the Graduate School of Engineering and the Global COE program of Tohoku University (Japan) for financial support. The authors are grateful to Prof. Wioleta Smiszek-Lindert, University of Slesia (Poland), for the generous gift of compound **BA**.

Supporting Information Available: Cartesian coordinates of the two lowest-energy conformers of capsaicin; scaling factors for the different types of vibrational internal coordinates. This material is available free of charge via the Internet at http://pubs.acs.org.

References and Notes

(1) Prasad, B. C. N.; Shrivastava, R.; Ravishankar, G. A. *Evidence-Based Integrative Med.* **2005**, *2*, 147.
(2) Binshtok, A. M.; Bean, B. P.; Woolf, C. J. *Nature* **2007**, *449*, 607.
(3) Surh, Y.-J.; Lee, S. S. *Life Sci.* **1995**, *55*, 1845.
(4) Walpole, C. S.; Wrigglesworth, R.; Bevan, S.; Campbell, E. A.; Dray, A.; James, I. F.; Perkins, M. N.; Reid, D. J.; Winter, J. *J. Med. Chem.* **1993**, *36*, 2362–2373.

(5) Hosseini, M.; Maddalena, D. J.; Spence, I. *J. Chem. Inf. Comput. Sci.* **1997**, *37*, 1129.
(6) Lambert, J. W.; Sum, A. K. *J. Phys. Chem. B* **2006**, *110*, 2351.
(7) David, W. I. F.; Shankland, K.; Shankland, N. *J. Chem. Soc. Chem. Commun.* **1998**, 931.
(8) Cornell, W. D.; Cieplak, P.; Bayly, C. I.; Gould, I. R.; Merz, K. M., Jr.; Ferguson, D. M.; Spellmeyer, D. C.; Fox, T.; Caldwell, J. W.; Kollman, P. A. *J. Am. Chem. Soc.* **1995**, *117*, 5179.
(9) Judson, R. S.; Rabitz, H. *Phys. Rev. Lett.* **1992**, *68*, 1500.
(10) *Sybyl 7.0*; Tripos Inc.: St. Louis, MO, 2004.
(11) Zhao, Y.; Truhlar, D. G. *J. Phys. Chem. A* **2004**, *108*, 6908.
(12) Wilson, E. B.; Decius, J. C.; Cross, P. C. *Molecular Vibrations*; McGraw-Hill: New York, 1945.
(13) (a) Keresztury, G.; Billes, F.; Kubinyi, M.; Sundius, T. *J. Phys. Chem. A* **1998**, *102*, 1731. (b) Nandini, G.; Sathyanarayana, D. N. *J. Mol. Struct. (theochem)* **2002**, *579*, 1. (c) Levin, I. W.; Pearce, R. A. R.; Harris, W. C. *J. Chem. Phys.* **1973**, *59*, 3048.
(14) Smiszek-Lindert, W.; Kusz, J. *Acta Crystallogr.* **2007**, *E63*, o3713.
(15) von Niessen, W.; Schirmer, J.; Cederbaum, L. S. *Comp. Phys. Rep.* **1984**, *1*, 57.
(16) Zakrzewski, V. G.; Ortiz, J. V. *Int. J. Quantum Chem.* **1995**, *53*, 583.
(17) Zakrzewski, V. G.; Ortiz, J. V.; Nichols, J. A.; Heryadi, D.; Yeager, D. L.; Golab, J. T. *Int. J. Quantum Chem.* **1996**, *60*, 29.
(18) Dunning, T. H., Jr *J. Chem. Phys.* **1970**, *53*, 2823.
(19) Stratmann, R. E.; Scuseria, G. E.; Frisch, M. J. *J. Chem. Phys.* **1998**, *109*, 8218.
(20) Woon, D. E.; Dunning, T. H., Jr. *J. Chem. Phys.* **1993**, *98*, 2823.
(21) Barone, V.; Cossi, M.; Tomasi, J. *J. Chem. Phys.* **1997**, *107*, 3210.
(22) Barone, V. Structure, Magnetic Properties and Reactivities of Open-Shell Species. In *Recent Advances in Density Functional Methods, Part I*; Chong, D. P., Ed.; World Scientific: Singapore, 1995.
(23) Frisch, M. J.; Trucks, G. W.; Schlegel, H. B.; Scuseria, G. E.; Robb, M. A.; Cheeseman, J. R.; Montgomery, J. A., Jr.; Vreven, T.; Kudin, K. N.; Burant, J. C.; Millam, J. M.; Iyengar, S. S.; Tomasi, J.; Barone, V.; Mennucci, B.; Cossi, M.; Scalmani, G.; Rega, N.; Petersson, G. A.; Nakatsuji, H.; Hada, M.; Ehara, M.; Toyota, K.; Fukuda, R.; Hasegawa, J.; Ishida, M.; Nakajima, T.; Honda, Y.; Kitao, O.; Nakai, H.; Klene, M.; Li, X.; Knox, J. E.; Hratchian, H. P.; Cross, J. B.; Bakken, V.; Adamo, C.; Jaramillo, J.; Gomperts, R.; Stratmann, R. E.; Yazyev, O.; Austin, A. J.; Cammi, R.; Pomelli, C.; Ochterski, J. W.; Ayala, P. Y.; Morokuma, K.; Voth, G. A.; Salvador, P.; Dannenberg, J. J.; Zakrzewski, V. G.; Dapprich, S.; Daniels, A. D.; Strain, M. C.; Farkas, O.; Malick, D. K.; Rabuck, A. D.; Raghavachari, K.; Foresman, J. B.; Ortiz, J. V.; Cui, Q.; Baboul, A. G.; Clifford, S.; Cioslowski, J.; Stefanov, B. B.; Liu, G.; Liashenko, A.; Piskorz, P.; Komaromi, I.; Martin, R. L.; Fox, D. J.; Keith, T.; Al-Laham, M. A.; Peng, C. Y.; Nanayakkara, A.; Challacombe, M.; Gill, P. M. W.; Johnson, B.; Chen, W.; Wong, M. W.; Gonzalez, C.; Pople, J. A. *Gaussian 03*, revision D.01; Gaussian, Inc.: Wallingford, CT, 2004.
(24) Klasinc, L.; Kovač, B.; Ruščić, B. *Kem. Ind. (Zagreb)* **1974**, *10*, 569.
(25) Sanche, L.; Schulz, G. J. *Phys. Rev. A* **1972**, *5*, 1672.
(26) Modelli, A.; Jones, D.; Distefano, G. *Chem. Phys. Lett.* **1982**, *86*, 434.
(27) Johnston, A. R.; Burrow, P. D. *J. Electron Spectrosc. Relat. Phenom.* **1982**, *25*, 119.
(28) Lucarini, M; Luppi, B.; Pedulli, G. F.; Roberts, B. P. *Chem. Eur. J.* **1999**, *5*, 2048.
(29) Ryu, S.; Liu, B.; Qin, F. *J. Gen. Physiol.* **2003**, *122*, 45.
(30) Nakamura, T.; Ooi, T.; Kogure, K.; Nishimura, M.; Terada, H.; Kusumi, T. *Tetrahedron Lett.* **2002**, *43*, 8181.
(31) Overend, J.; Scherer, J. R. *J. Chem. Phys.* **1960**, *32*, 1289.
(32) *The Aldrich Library of FT-IR Spectra*, 2nd ed.; Sigma-Aldrich Co., 1997.
(33) Sweigart, D. A.; Turner, D. W. *J. Am. Chem. Soc.* **1972**, *94*, 5592.
(34) Masclet, P.; Grosjean, D.; Mouvier, G.; Dubois, J. *J. Electron Spectrosc. Relat. Phenom.* **1973**, *2*, 225.
(35) Jacques, P.; Allonas, X.; Burget, D.; Haselbach, E.; Muller, P.-A.; Sergenton, A.-C.; Galliker, H. *Phys. Chem. Chem. Phys.* **1999**, *1*, 1867.
(36) Deleuze, M. S. *J. Chem. Phys.* **2002**, *116*, 7012.
(37) Deleuze, M. S. *J. Phys. Chem. A* **2004**, *108*, 9244.
(38) Deleuze, M. S. *Chem. Phys.* **2006**, *329*, 22.
(39) Simons, J.; Jordan, K. D. *Chem. Rev.* **1987**, *87*, 535.
(40) Dunning, T. H., Jr.; Peterson, K. A.; Woon, D. E. Basis Sets: Correlation Consistent Sets. In *Encyclopedia of Computational Chemistry*; Schleyer, P. v. R., Ed.; Wiley: Chichester, UK, 1998.
(41) Chen, D.; Gallup, G. A. *J. Chem. Phys.* **1990**, *93*, 8893.
(42) Staley, S. S.; Strnad, J. T. *J. Phys. Chem.* **1994**, *98*, 161.
(43) Chao, J. S-Y.; Falcetta, M. F.; Jordan, K. D. *J. Chem. Phys.* **1990**, *93*, 1125.
(44) Burrow, P. D.; Howard, A. E.; Johnston, A. R.; Jordan, K. D. *J. Phys. Chem.* **1992**, *96*, 7570.
(45) Venuti, M.; Modelli, A. *J. Chem. Phys.* **2000**, *113*, 2159.
(46) Modelli, A.; Hajgató, B.; Nixon, J. F.; Nyulászi, L. *J. Phys. Chem. A* **2004**, *108*, 7440.
(47) Modelli, A. *Phys. Chem. Chem. Phys.* **2003**, *5*, 2923.
(48) Modelli, A. *Trends Chem. Phys.* **1997**, *6*, 57.
(49) Galasso, V.; Kovač, B.; Modelli, A.; Ottaviani, M. F.; Pichierri, F. *J. Phys. Chem. A* **2008**, *112*, 2331.
(50) Jordan, K. D.; Burrow, P. D. *Chem. Rev.* **1987**, *87*, 557.
(51) Modelli, A.; Distefano, G.; Jones, D. *Chem. Phys.* **1982**, *73*, 395.
(52) Jordan, K. D.; Burrow, P. D. *J. Am. Chem. Soc.* **1980**, *102*, 6882.
(53) Kogure, K.; Goto, S.; Nishimura, M.; Yasumoto, M.; Abe, K.; Ohiwa, C.; Sassa, H.; Kusumi, T.; Terada, H. *Biochim. Biophys. Acta* **2002**, *1573*, 84.
(54) Gannett, P. M.; Nagel, D. L.; Reilly, P. J.; Lawson, T.; Sharpe, J.; Toth, B. *J. Org. Chem.* **1988**, *53*, 1064.
(55) Dearden, J. C.; Forbes, W. F. *Can. J. Chem.* **1956**, *27*, 1294.
(56) Kwasniewski, S. P.; Deleuze, M. S.; François, J. P. *Int. J. Quantum Chem.* **2000**, *80*, 672.
(57) Hsu, C.-P.; Hirata, S.; Head-Gordon, M. *J. Phys. Chem. A* **2001**, *105*, 451.
(58) Fau, S.; Bartlett, R. J. *J. Phys. Chem. A* **2003**, *107*, 6648.
(59) *Calculation of NMR and EPR Parameters*, Kaupp, M., Bühl, M., Malkin, V. G., Eds.; Wiley-VCH: Weinheim, 2004.
(60) Rogowska, A.; Kuhl, S.; Schneider, R.; Walcarius, A.; Champagne, B. *Phys. Chem. Chem. Phys.* **2007**, *9*, 828.
(61) Holton, D. M.; Murphy, D. *J. Chem. Soc., Faraday Trans. I* **1982**, 1223.
(62) Joela, H.; Kasa, S.; Mäkelä, R.; Salo, E.; Hannonen, K. *Magn. Reson. Chem.* **1990**, *28*, 261.
(63) Stone, T. J.; Waters, W. A. *J. Chem. Soc.* **1964**, 213.
(64) Ulmschneider, K. B.; Stegmann, H. B. In *Landolt-Börnstein, new series: Magnetic properties of free radicals*; Fischer, H., Hellwege, K.-H., Eds.; Springer, 1980; 9/d1.
(65) Jones, M. T. In *Landolt-Börnstein, new series: Magnetic properties of free radicals*; Fischer, H., Ed.; Springer, 1988; 17/f.
(66) Klotz, D.; Jülicj, Th.; Wex, J.; Stegmann, H. B. In *Landolt-Börnstein, new series: Magnetic properties of free radicals*; Fischer, H., Ed.; Springer, 1989; 17/g.
(67) Klotz, D.; Deuschle, G.; Wex, J.; Stegmann, H. B. In *Landolt-Börnstein, new series: Magnetic properties of free radicals*; Fischer, H., Ed.; Springer, 1988; 17/e.
(68) Valentine, J. S.; Curtis, A. B. *J. Am. Chem. Soc.* **1975**, *97*, 224.
(69) Lown, J. W. In *Anthracycline and anthracenedione-based anticancer agents*; Elsevier: Amsterdam, 1988.
(70) Alberti, A; Bolognese, A.; Guerra, M.; La Vecchia, A.; Macciantelli, D.; Marcaccio, M.; Novellino, E.; Paolucci, F. *Biochemistry* **2003**, *42*, 11924.

JP801890G